2024 IEEE/RSJ International Conference on Intelligent Robots and Systems (IROS)
October 14-18, 2024. Abu Dhabi, UAE

The design of a sensorized laryngoscope training system for pediatric intubation

Ningzhe Hou[1*] , Liang He[2], Alessandro Albini[1], Louis Halamek[3] and Perla Maiolino[1,4]

***Abstract*— Intubation is essential for ventilating critically ill patients and involves precise maneuvering of a laryngoscope to place an endotracheal tube (ETT). However, training for this procedure is fraught with challenges. Traditional methods, relying on manikins or training with a single sensing modality, fail to adequately convey important interaction information. Such challenge is heightened in pediatric intubation due to anatomical differences that demand greater precision. Furthermore, integrating multiple sensing modalities into a laryngoscope without changing its size presents a significant design challenge, critical for maintaining realistic training scenarios. To overcome these obstacles, we developed a sensorized laryngoscope system equipped with a force-torque sensor, a 9-axis inertial measurement unit (IMU), and tactile sensors. This system, validated in a preliminary user study, provides online feedback on angles, forces, and grip strength through an online feedback GUI. Adopting a learning-by-demonstration approach with both experts and novices, the initial validation confirmed the system's potential, paving the way for expanded trials with more participants.**

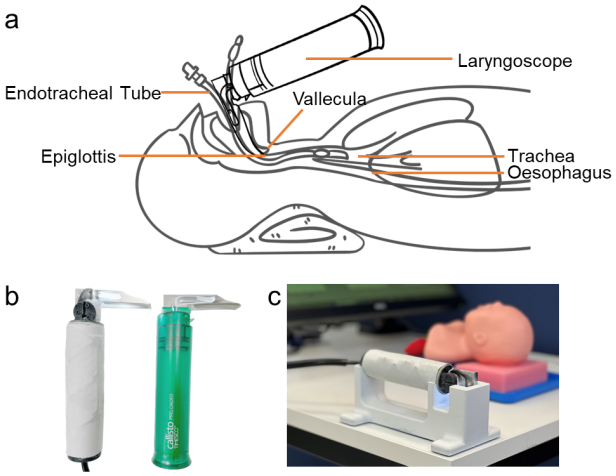

Fig. 1. (a) The illustration of tracheal intubation. (b) The sensorised laryngoscope (left) compares to the Callisto (Miller) laryngoscope. (c) The training system.

I. INTRODUCTION

Intubation, involving the insertion of an endotracheal tube into the trachea via the mouth or nose, ensures direct lung ventilation for oxygen delivery. It is essential for maintaining an open airway under general anesthesia and in emergencies like respiratory failure, drug overdoses, or severe trauma[1].

Direct laryngoscopy is a medical procedure that is widely employed for tracheal intubation, wherein a laryngoscope — a specialized instrument with a light source — is inserted into the patient's mouth to visualize the larynx directly. The process begins with the patient being appropriately positioned[2] to aligns the oral, pharyngeal, and laryngeal axes, thus facilitating the passage of the ETT. After appropriate sedation and muscle relaxation[3], the laryngoscope's blade is gently introduced into the mouth. As the blade is advanced, the epiglottis comes into view, which is either directly lifted by the blade or indirectly elevated by positioning the blade into the vallecula (as shown in Figure 1a). Once the vocal cords are visualized, an endotracheal tube is carefully advanced between them and into the trachea to ensure a patent airway. Proper placement is then confirmed using a variety of methods, including auscultation and end-tidal carbon dioxide detection.

Laryngoscope intubation training poses challenges for healthcare professionals. One of the primary difficulties faced during intubation is achieving a clear view of the vocal cords with the laryngoscope, which may be obscured by anatomical variations[4]. Additionally, repeated attempts at intubation can lead to tissue trauma, swelling, and increased risk of more serious complications[5], making the first-pass success crucial. One study [6] revealed that 51.2% of the patients suffer from a certain level of injuries after laryngoscopy. Another challenge is the potential for aspiration[7], especially in non-fasting patients or those with gastric reflux. In emergency scenarios, external factors like limited time, patient non-cooperation, and the presence of cervical spine injuries[8] can also heighten the challenges of successful intubation.

Intubation for pediatric patients is particularly challenging, primarily due to the proportionally larger tongue, differently shaped larynx[9][10], small cricothyroid membrane, and more fragile tissue[11].

Despite recent advancements in robotic-assisted intubation, such as the IntuBot[12], REALITI system[13], and a remote robot-assisted intubation system (RRAIS)[14], none have entered clinical trials due to the procedure's complexity and the systems' inability to handle patient-specific variations. These innovations show promise in pre-clinical settings, including improved success rates in animal experi-

This work was supported by the Engineering and Physical Sciences Research Council (EPSRC) Grant EP/V000748/1; Dr. Halamek's contribution was supported by the Endowment for the Center for Advanced Pediatric and Perinatal Education.

[1]Oxford Robotics Institute, University of Oxford, UK; [2]Institute of Biomedical Engineering, University of Oxford, UK; [3]Department of Pediatrics, Stanford University, USA; [4]University of Genoa, Liguria, IT;
*Corresponding Author: Ningzhe Hou
ningzhe.hou@eng.ox.ac.uk

ments. However, the precision and adaptability required for endotracheal intubation mean that human expertise remains essential. The gap between robotic capabilities and the demands of real-world clinical application highlights the ongoing need for human training in this critical medical procedure.

Video laryngoscopes such as Pentax-AWS have been demonstrated to enhance the success rate of intubation and reduce the time required compared to the traditional direct laryngoscope [15]. However, video laryngoscopes lack force and torque feedback, crucial for preventing tissue damage, and the availability of video laryngoscopes, especially in emergency scenarios, poses additional challenges.

Previous research highlights that both observable and unobservable factors significantly impact the learning and execution of intubation techniques, affecting how novices and experts differ in their grip gestures and laryngoscope angles [16]. Traditional training methods used by experts, though beneficial, are limited in conveying the complex, unobservable aspects of the procedure. These include the nuanced interplay of tactile forces between the operator's hand, the laryngoscope handle, and the oral cavity, as well as the critical, yet unobservable, forces and torque on tissues that are key to avoiding tissue damage [17]. Such complexity poses challenges for novices in precisely replicating the sophisticated techniques of experts, which involve specific grips and positioning of the laryngoscope. In this context, "seen" elements refer to actions that are directly observable, such as grip gestures and laryngoscope angles, while "unseen" elements include forces, torques, and tactile interactions crucial for mastering intubation. Communicating these essential, yet unobservable, elements effectively through verbal instructions and demonstrations remains a substantial challenge in training programs.

Recent advancements in robotics and sensor technology are revolutionizing intubation training by enabling the precise measurement of critical seen and unseen factors. Intelligent training tools, such as the Waseda-Kyotokagaku Airway No. 1R (WKA-1R), mimic human anatomy with high fidelity and incorporate sensors for objective feedback on the forces applied during intubation. These innovations allow for a quantitative evaluation of trainees' performance, helping distinguish expertise levels through discriminant analysis. Additionally, sensorized training phantoms equipped with vibrotactile feedback provide real-time data on force vectors, significantly improving skill retention and reducing unwanted force application. This leap in training technology promises enhanced learning outcomes, offering an objective, data-driven approach to mastering the complexities of intubation [18][19].

Several laryngoscope integrated with individual sensors, such as force and torque sensor[20][21] and IMU[22] have also previously been developed. However, considering the complexity and interrelation of these parameters, relying on sensing data from only a subset complicates novices' ability to gain a holistic understanding of actions, which involving

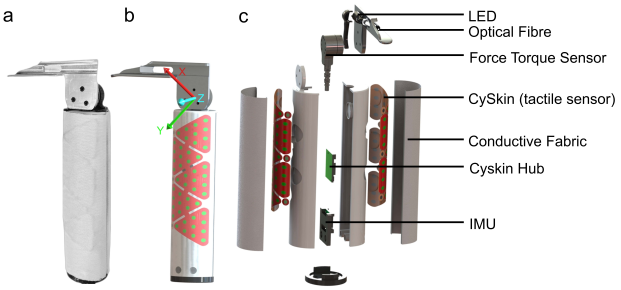

Fig. 2. (a) The image of the sensorised laryngoscope. (b) The positions of tactile sensors and Force/Torque Sensor sensing direction. (c) An exploded view of the inner details of the laryngoscope.

a wide range of parameters. Integrating all necessary sensors into a single laryngoscope without altering its diameter and size poses a significant challenge. A training setup that differs from the real-world scenario might not be as effective, and currently, there is no single laryngoscope training setup that encompasses all these parameters.

To address this issue, we have developed a sensorized laryngoscope modeled after the Callisto (Miller) laryngoscope (Figure 1b), the most commonly used laryngoscope for pediatric intubation. This laryngoscope can measure three-axis force and torque applied to the manikin, absolute Euler angles, as well as capture tactile data such as grip gestures and pressure. In addition, we introduced a graphical user interface (GUI) training system that synchronizes all the quantified parameters and can be utilized for feedback during training sessions. We devised a preliminary experiment to initiate the verification of the system's functionality. Both expert and novice subjects were invited to engage in a learning-by-demonstration approach for the study, where the experts' data were collected and analyzed to serve as the gold standard in guiding novice operators.

II. Hardware and Software Architecture Design

A. Hardware architecture

As shown in the exploded view in Figure 2c, the sensorised laryngoscope consists of 4 parts: a nine-axis IMU(GY-95T Guangyun Electronics), CySkin distributed tactile sensors[23] covered with conductive fabric, 6-axis F/T sensor(Nano 17, ATI Industrial Automation), and a LED (C503D-WAN-CCbEb151, Cree) connected with optical fibre. The main body of laryngoscope is designed by SolidWorks and 3D printed with VeroWhite Plus by a Stratasys J735 3D printer(Stratasys, Ltd.).

A 9-axis IMU, inclusive of a 3-axis magnetometer, was chosen for its ability to provide a stable reference by sensing the Earth's magnetic field, thereby mitigating drift errors in gyroscope and accelerometer readings. This ensures precise and reliable orientation estimations during intubation, where even a slight drift can substantially affect the outcome.

The Nano 17 6-axis F/T sensor provides a maximum force measurement of $50\,\mathrm{N}$ in both the x and y axes, and $70\,\mathrm{N}$ in the z axis. Additionally, it offers a torque measurement of $500\,\mathrm{Nmm}$ across all three axes. The sensor boasts a resolution of $1/80\,\mathrm{N}$ for force and $1/16\,\mathrm{Nmm}$ for torque.

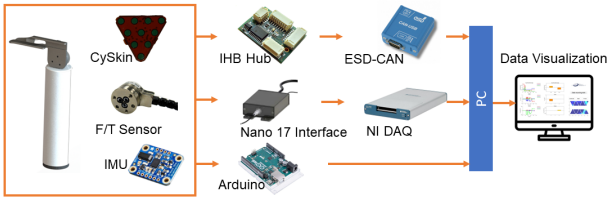

Fig. 3. The hardware architecture of the laryngoscope.

The X and Y axes of the Force Torque sensor do not align with the handle direction; instead, there is a 30-degree rotation due to the sensor's design, as shown in Figure 2b. Since force and torque measurements are highly dependent on the setup and thus there is no existing literature to reference, we conducted preliminary experiment with experts to ensure that both the measuring range and resolution met the requirements.

Ten rectangular CySkin patches are applied to the laryngoscope, with each patch containing ten tactile sensing points. This results in a total of 100 pressure sensing points that encompass the handle of the laryngoscope (Figure 2b). The extensive pressure distribution is well-suited for recognizing grip gestures.

A 5-mm round LED, with a luminous intensity of 64.6 cd, is deployed to provide ample illumination without causing discomfort or harm to the operator's eyes. To ensure optimal visualization of the larynx, this light is channeled to the blade's tip via a 5mm optical fibre.

The system integration (Figure 3) leverages various techniques for data processing and communication. The CySkin patches utilize the I2C protocol for communication between patches. These patches are subsequently linked to the IHB Hub, where data processing takes place. After processing, the data is transmitted via the CAN Bus. A subsequent CAN-USB Interface, provided by ESD Electronics gmbh, converts the CAN bus signals to USB, enabling the data to be forwarded to a laptop for additional processing and vitalization.

The F/T sensor connects to the Nano 17 Interface (9105-IFPS-1, ATI Industrial Automation) to generate analog voltage signals, captured by the DAQ system (USB-6363, National Instrument). Utilizing NI support packages in MATLAB, these signals are transformed into force and torque values using the Runtime Matrix supplied by the manufacturer for each sensor. These values are further refined using a setup-specific calibration matrix. The IMU interacts with an Arduino UNO through the I2C bus. 9-axis data are processed locally in Arduino UNO to derive absolute pitch, roll, and yaw angles through Complementary Filter, which are then sent to a laptop for further processing.

B. Software architecture

Given the diverse sources of measurements with varying sampling rates, asynchronous data reading is employed to allow each sensor to write to its own buffer, while an interrupt is triggered by incoming new data. The system updates at a relatively constant rate by accessing the most recent data from all sensors. This rich set of quantified parameters is central to deepening operational understanding and speeding up the learning curve. Leveraging a learning-by-demonstration framework, this study seeks to validate the usability of the proposed sensorized laryngoscope. Through comprehensive analysis of data gathered from numerous trials conducted by a substantial pool of experts, the maximum and minimum values recorded by each sensor during these expert trials are discerned. These values serve as benchmarks for subsequent evaluations, helping to guide and shape the behavior of the novices.

For each sampled measurement of certain sensing modality in a trail, an error will be generated if the measurement exceeds the maximum standard value or falls below the minimum standard value. Let $M(t)$ = measurement, $S_{\max}$ = maximum standard value, and $S_{\min}$ = minimum standard value extracted from expert demonstration. The normalised error for each measurement $E_{\text{norm}}(t)$ can be estimated as a function of measurement $M(t)$, upper and lower measuring range of of the sensor Max and Min:

$$\mathrm{E}_{\text{norm}}(t) = \begin{cases} \frac{M(t)-S_{\max}}{\text{Max}-S_{\max}}, & \text{if } M > S_{\max} \\ \frac{M(t)-S_{\min}}{\text{Min}-S_{\min}}, & \text{if } M < S_{\min} \\ 0, & \text{otherwise} \end{cases}$$

To evaluate performance, it is essential to establish an Error Point P that imposes penalties based on the errors detected by each sensor. Aggressive movements are more likely to cause tissue damage compared to slower, low-error motions. However, since the derivative of error is inadequate for quantifying the aggressiveness of a motion, the system's sensitivity to errors must be adjustable. This ensures that higher errors incur exponentially higher penalties. To address this, we have incorporated a method from the Risk-Sensitive Reinforcement Learning Framework [24]. In our case, this means that the relationship between error and penalty is not linear but exponential, resulting in exponentially higher penalties for aggressive motions. The expression of the Error Point P for each individual sensor can be expressed as

$$\mathrm{P}_{Sensor} = \sum_{S_1}^{S_n} \left(w_{S_x} \int_{t_0}^{t_n} e^{kE_{\text{norm}}(t)} - 1 \, dt \right)$$

in which S_n represents distinct parameters within the same modality. For example, the IMU measures errors along the x, y, and z axes. The term w_{S_x} signifies the weighting assigned to each measurement within this sensing modality. Measurements deemed more critical should be allocated higher weightings, thereby exerting greater influence on the overall score, and vice versa. An exponential function, incorporating the adjustable parameter k, is employed to penalize larger errors more severely than smaller ones.

A Score S is calculated based on the Error Point of each sensor and time as an overall evaluation of the trail:

$$\text{Score} = P_{\text{IMU}} + P_{\text{Torque}} + P_{\text{Force}} + \lambda(t_n - t_0)$$

The variable λ denotes the importance of the time penalty in the comprehensive evaluation, emphasizing that completion

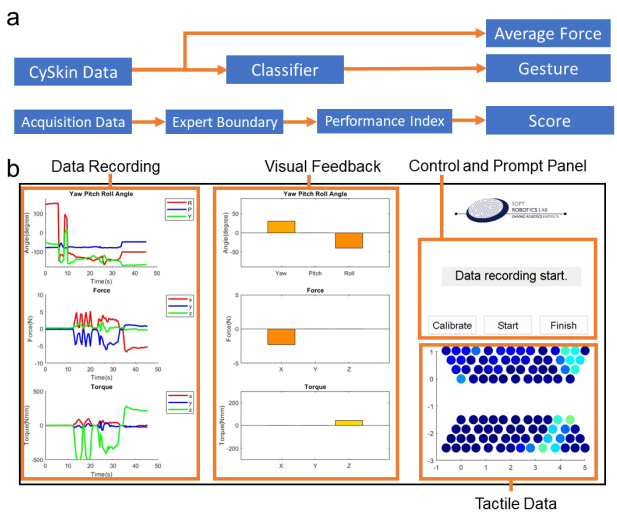

Fig. 4. (a) Software architecture flowchart. (b) A screenshot of the GUI designed for training.

time is a vital aspect of intubation, especially for pediatric intubations and emergency scenarios [25].

The acquisition system's GUI is depicted in Figure 4b and encompasses four main components. On the left are three plots that provide visualization and recording of the measurements. Adjacent to this, in the middle column, are three plots dedicated to error indications. These error bars will show up if measurements either exceed the maximum or fall below the minimum set values. When errors are detected, the corresponding error bar will display the extent of the deviation. A more pronounced error results in a darker red error bar, serving as a visual cue for the novice. This feedback mechanism via the error bar plays a pivotal role in prompting novices to adjust their movements accordingly.

The visualization of CySkin shows in right corner of the GUI, showcasing the tactile image resulting from the grip on the laryngoscope. Directly above the CySkin data is the "Control and Prompt Panel", which governs the training sequence. At the commencement of each training session, the laryngoscope must be positioned in its holding stand for calibration. The process ensures the IMU is drift-free (failure occurs with over 1-degree drift) and all sensors initialize correctly. After successful calibration, the user starts the intubation with the "Start" button, and upon completion, clicks "Finish". The score is then displayed, and data is saved for analysis.

III. Experimental Setup and Protocols

An experiment was designed to assess the functionality of the subsystem. This study has received approval from the Central University Research Ethics Committee (CUREC) of the University of Oxford (Approval Reference: R76888/RE001). The experimental setup is shown in Figure 5a. The setup includes: a neonatal manikin for pediatric intubation training, a monitor with adjustable viewing angle to provide visual feedback, a laryngoscope with the stand fixed on the table, and a pediatric ETT.

TABLE I

Expert Standards for Angle, Force and Torque

Measurement	Standard Max	Standard Min
Pitch	64.8°	0°
Roll	15.16°	-3.97°
Yaw	13.57°	-63°
Fx	4.31 N	-3.76 N
Fy	1.53 N	-4.21 N
Fz	1.16 N	-1.38 N
Tx	66.9 Nmm	-28.31 Nmm
Ty	79.73 Nmm	-47.79 Nmm
Tz	15.53 Nmm	-370.65 Nmm

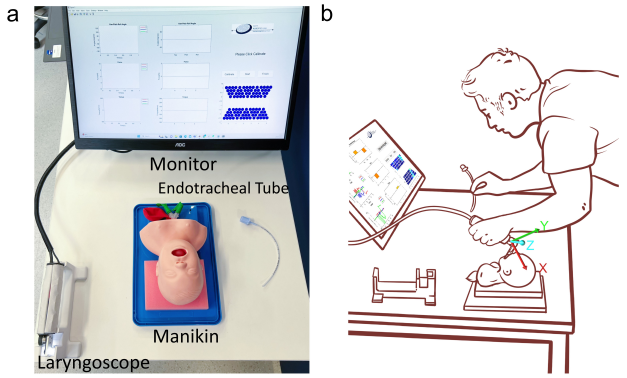

Fig. 5. (a) The experimental setup. (b) The illustration of a subject performing the intubation, with the force torque direction indicated.

A. Benchmarking and protocols

Firstly, three licensed physicians with at least three years of clinical experience in pediatric intubation, were enlisted to use the sensorized laryngoscope to establish performance standards for the subjects. Each performed intubation on the manikin 20 times (10 for each grip gesture), with 3-minute breaks in between trials. The data gleaned from these expert trials was subsequently analyzed to define the gold standard for the training system. The standard for each measurement is presented in Table 1. It should be noted that the validation of these standards is currently limited to three invited experts to initially assessed the proposed setup's functionality. A more robust benchmarking would necessitate analyzing data from a broader pool of experts.

A total of 3 subjects who had no experience in intubation were recruited, all of whom are right-handed (verified by a Handedness Screening Survey) and have no history of hand or arm injuries.

Before starting, subjects viewed a video tutorial on intubation covering both grasping methods, with the opportunity to practice using a laryngoscope on a manikin. During training, a GUI on a monitor offered visual feedback, and scores were given after each trial. Post-video, subjects selected their preferred grip gesture for the experiment, which remained unchanged throughout the trials. Each subject was asked to perform 10 trials consecutively, with a 3-minute break between each intubation. Successful insertion of the endotracheal tube into the lung marked the completion of a trial. The initial trial served as a pilot run and was not scored. Subsequently, every set of 3 trials constituted a stage for

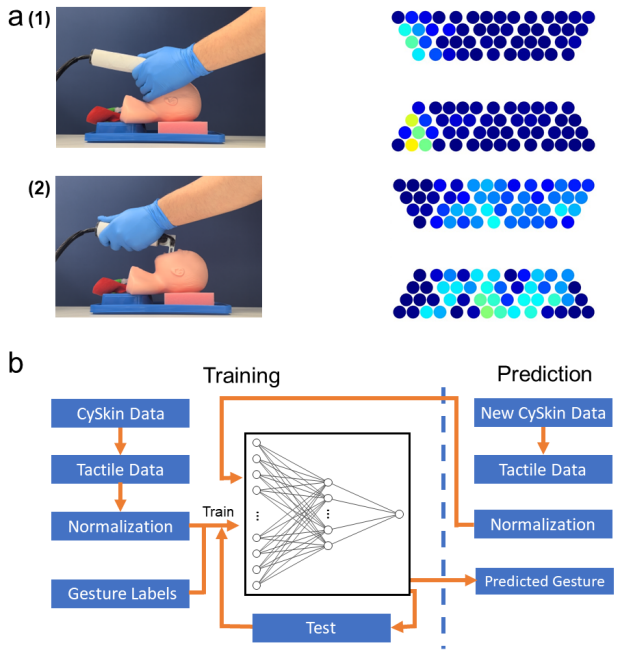

Fig. 6. (a) Two different grip gestures and examples of corresponding tactile patterns. (b) The classifier training architecture.

evaluation: trials 2-4 formed stage one, trials 5-7 formed stage two, and trials 8-10 formed stage three. After all the trials, all subjects were asked to provide written open-ended feedback on the training system.

To facilitate further analysis and fine-tuning, the weighting w_{S_x} for all sensors was set to 1, indicating uniform weighting across sensors. The parameter for the error's exponential penalty, k, is set to 1.1, indicating exponential growth in the penalty up to a maximum of 2.004 as the normalized error approaches a maximum of 1.

B. Gesture Recognition

Two primary grip gestures are commonly employed for pediatric intubation. The first method involves grasping the laryngoscope between the thumb and index finger, with the remaining fingers placed on the jaw of manikin, positioning the hand to manipulate the laryngoscope, as depicted in Figure 6a(1). The alternative method requires grasping the laryngoscope with all fingers, ensuring the thumb is aligned with the handle, as illustrated in Figure 6a(2). Since each grip gesture produces a distinct tactile pattern (right side of Figure 6a), all frames of the expert tactile patterns are labeled and used to train a neural network, enabling grip gesture recognition in the training system.

All tactile data were provided in arrays consisting of 100 elements each, representing readings from 100 pressure-sensing points. The data were normalized to a range between 0 and 1 and labeled with a binary classification: either 1 or 2. Following pre-processing, the data were randomly divided into a training set and a validation set according to a 70-30 split.

The training utilized a neural network architecture equipped with an input layer of 100 neurons (corresponding to the 100 data points of each sample), followed by two hidden layers containing 10 neurons each, and an output layer composed of 2 neurons to mirror the binary classification system. The Levenberg-Marquardt backpropagation algorithm facilitated the network's training process, with performance continually assessed through the calculation of the mean squared error (MSE) between the network's predictions and the actual target labels.

Upon completion of the training process, incoming CySkin data from subjects are classified by the well-trained network to identify the corresponding grip gestures. This classification hinges on determining the confidence that a given input aligns with one of the two established classes.

TABLE II
THE RESULT OF NEURAL NETWORK CLASSIFICATION

Subject	1	2	3
Gesture Used	2	1	1
Classification Result	2	1	1

IV. Experimental Results

As previously mentioned, the Score S calculated based on the Error Point of each sensing modality is a key metric for evaluating subjects' performance. A decrease in the score indicates an enhancement in performance and the impact of regulating subjects' actions.

Figure 7 illustrates that the overall score, along with its variance, decreased significantly over successive trials for all subjects. In terms of individual components, time and torque penalties demonstrated a substantial decline for each subject. Although the reduction in Euler angle penalties was not significant for subjects 2 and 3, subject 1 exhibited a notable decrease. The force penalties started off small and did not show a large reduction. The right column of the figures presents the composition percentages of different performance metrics as part of the overall score, along with their standard deviations. For Subject 1, the percentage contribution of time to the overall score is the most significant, followed by torque and force. Euler angle contributions are comparatively minor. Subjects 2 and 3 show a similar distribution, with time and torque being major contributors to the overall score, while Euler angle and force have lesser impacts. The standard deviation bars indicate variability in the measurements, with some metrics like time and Z Torque showing more variability in their contribution to the overall score across trials. The high standard deviations observed for time and Z Torque points, particularly in the case of Subject 1, correlate with the substantial reduction in these components seen in the left column. This suggests a greater variability in performance for these metrics at the outset, which then decreased over the course of the trials, indicating an improvement in consistency and technique. For Subjects 2 and 3, while the reductions in Euler angle and force points are less pronounced, the standard deviations are also smaller, implying a more consistent performance in these areas from the beginning of the trials.

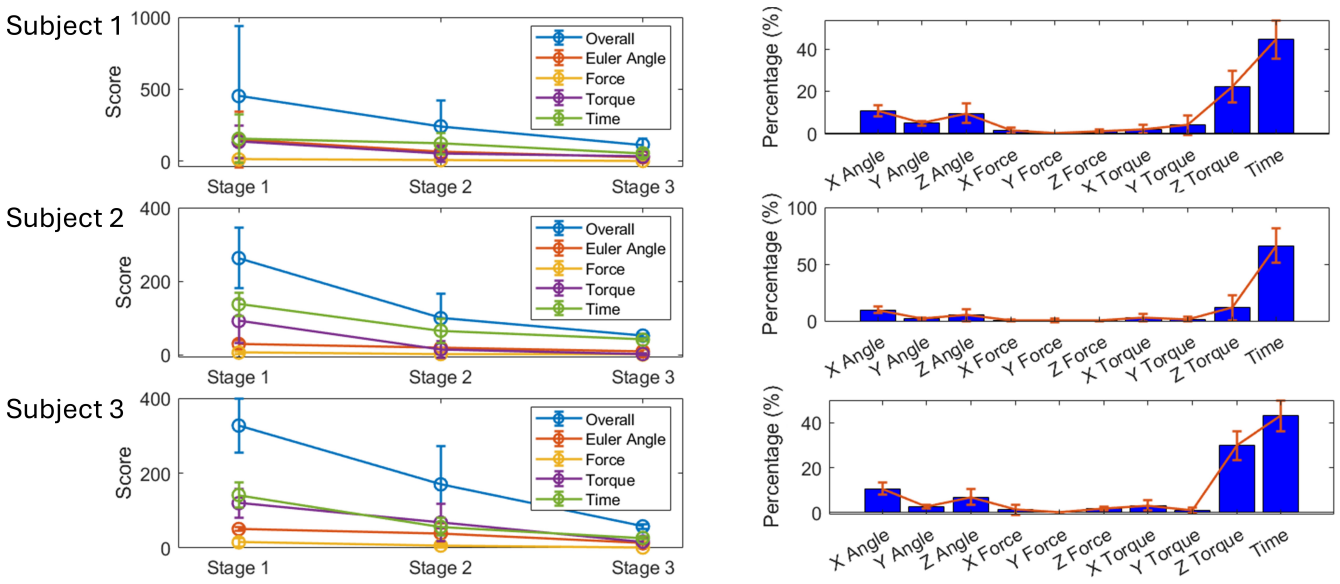

Fig. 7. Subject performance. Reduction in Overall Score, Euler Angle Point, Force Point, Torque Point, and Time Points between stages for each subject are on the left. The average composition percentages of different penalty points within the overall score, along with the standard deviation, are on the right.

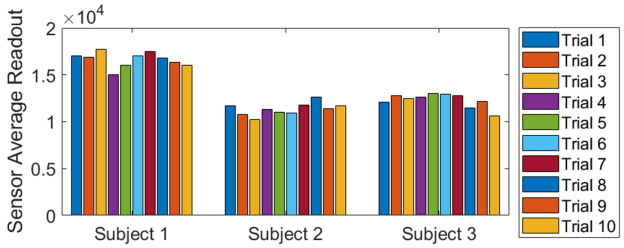

Fig. 8. Average tactile sensor values per trial in each subject.

The average grasping pressure is also interesting to investigate along with the classification result in Table II. The average pressure is calculated by determining the mean pressure across all the pressure-sensing points covered by the finger (the points where the readout differs by more than 500 compared to the resting state). As shown in Figure 8, no significant trends are observable across the various trials for individual subjects; the average pressure fluctuates without any consistent increase or decrease. The classification results of the holding gesture agree with the gestures adopted by the subjects. It is observable that the subject who adopted gesture 2 (Subject 1) exerted a relatively higher average pressure compared to those who adopted gesture 1 (Subjects 2 and 3). This variation merits further investigation with a larger cohort of subjects.

In the experiment feedback, subjects found the sensors and error indicators beneficial for task completion but noted areas for improvement. The error feedback was not intuitive, making it difficult to adjust techniques effectively. Additionally, the challenge of dividing attention between the screen and the larynx, due to the limited visual space and strict angle requirements, was significant. Two subjects also reported eye strain, attributed to high brightness of the optical fiber used.

V. Conclusion and Future Work

In conclusion, this study addresses the tracheal intubation training challenges faced by novice healthcare professionals by presenting a sensor-equipped laryngoscope that quantifies key visible and invisible parameters. These parameters encompass absolute Euler angles of the laryngoscope, forces, torques, and tactile hand interactions. The hardware integration and software synchronization of the sensorized laryngoscope consisted of a myriad of components including a nine-axis IMU, distributed tactile sensors, a 6-axis F/T sensor, and an LED coupled with an optical fiber.

A user study was conducted to validate the system's functionality. Although the experiment had a limited number of subjects, the findings showed the system's effectiveness in measuring behavioral parameters during training, providing useful insights for future, more comprehensive studies. The study indicated that visual feedback presented on a monitor can guide the trainees' actions during intubation training. However, while this feedback can accelerate skill acquisition, it may also lengthen the total time for intubation as subjects reported difficulty in alternating their attention between the manikin and the monitor. To streamline the process, the use of AR glasses could be considered to provide visual error feedback directly within the user's field of view, eliminating the need to shift focus. An alternative choice is providing the visual feedback to a trainer to remind the novice during the experiment.

In the next phase, following the resolution of hardware and GUI issues highlighted in this paper, the experiment will be extended to a broader cohort of participants, including both novices and experts. Based on the experimental outcomes, parameters such as w_{S_x} and k will be refined using an optimization algorithm like gradient descent, directed by an objective function focused on maximizing the rate of

learning improvement. As the tactile dataset from experts expands, we will also be able to conduct more detailed classification analyses on specific parameters in the gripping. Ultimately, our goal is to conduct a large-scale study with a substantial pool of subjects to evaluate the system's efficacy.

REFERENCES

[1] C. A. Hagberg, C. A. Artime, and M. F. Aziz. *Hagberg and Benumof's Airway Management*. 4th ed. Elsevier, 2020.

[2] R. D. Miller et al. *Miller's Anesthesia*. 8th ed. Philadelphia: Elsevier Saunders, 2015.

[3] G. E. Morgan, M. S. Mikhail, and M. J. Murray. *Clinical Anesthesiology*. McGraw-Hill, 2013.

[4] R. M. Levitan et al. "The complexities of tracheal intubation With direct laryngoscopy and alternative intubation devices". In: *Annals of Emergency Medicine* 57.3 (2011), pp. 240–247. ISSN: 0196-0644.

[5] P. C. Pacheco-Lopez et al. "Complications of airway managementdiscussion". In: *Respiratory Care* 59.6 (June 2014), pp. 1006–1021.

[6] J. Mourão et al. "Soft tissue injuries after direct laryngoscopy". In: *Journal of Clinical Anesthesia* 27.8 (Dec. 2015), pp. 668–671.

[7] B. E. Driver et al. "The occurrence of aspiration pneumonia after emergency endotracheal intubation". In: *The American Journal of Emergency Medicine* 36.2 (Feb. 2018), pp. 193–196.

[8] M. C. Gerling et al. "Effects of cervical spine immobilization technique and laryngoscope blade selection on an unstable cervical spine in a cadaver model of intubation". In: *Annals of Emergency Medicine* 36.4 (2000), pp. 293–300. ISSN: 0196-0644.

[9] J. S. Doherty, S. R. Froom, and C. D. Gildersleve. "Pediatric laryngoscopes and intubation aids old and new". In: *Pediatric Anesthesia* 19.s1 (2009), pp. 30–37.

[10] E. Long, S. Sabato, and F. E. Babl. "Endotracheal intubation in the pediatric emergency department". In: *Pediatric Anesthesia* 24.12 (2014), pp. 1204–1211.

[11] R. M. Walls et al. *The Walls Manual of Emergency Airway Management*. Lippincott Williams & Wilkins, 2021.

[12] X. Cheng et al. "IntuBot: Design and prototyping of a robotic intubation device". In: *2018 IEEE International Conference on Robotics and Automation (ICRA)*. 2018, pp. 1482–1487.

[13] Q. Boehler et al. "REALITI: A robotic endoscope automated via laryngeal imaging for tracheal intubation". In: *IEEE Transactions on Medical Robotics and Bionics* 2.2 (2020), pp. 157–164.

[14] X. Wang, Y. Tao, X. Tao, et al. "An original design of remote robot-assisted intubation system". In: *Scientific Reports* 8 (2018), p. 13403.

[15] Y. Sakurai and M. Tamura. "Efficacy of the Airway Scope (Pentax-AWS) for training in pediatric intubation". In: *Pediatrics International* 57.2 (2015), pp. 217–221.

[16] J. E. Zamora, B. J. Weber, A. R. Langley, et al. "Laryngoscope manipulation by experienced versus novice laryngoscopists". In: *Canadian Journal of Anesthesia/Journal canadien d'anesthésie* 61 (2014), pp. 1075–1083.

[17] M. Carassiti et al. "Force and pressure distribution using Macintosh and GlideScope laryngoscopes in normal and difficult airways: a manikin study". In: *BJA: British Journal of Anaesthesia* 108.1 (Sept. 2011), pp. 146–151. ISSN: 0007-0912.

[18] H. Zhou et al. "A method to use haptic feedback of laryngoscope force vector for endotracheal intubation training". In: *2023 IEEE International Conference on Robotics and Automation (ICRA)*. 2023, pp. 6810–6816.

[19] Y. Noh et al. "Development of the evaluation system for the Airway Management Training System WKA-1R". In: *2008 2nd IEEE RAS & EMBS International Conference on Biomedical Robotics and Biomechatronics*. 2008, pp. 574–579.

[20] G. M. Rao et al. "Design, development, and face validation of an intubation simulation device using real-time force data feedback". In: *Laryngoscope Investigative Otolaryngology* 7.5 (2022), pp. 1506–1512.

[21] P. McWilliam et al. "Sensor-Integrated laryngoscope: A key step toward safe neonatal intubation". In: *Journal of Clinical Engineering* 45.1 (Jan. 2020), pp. 39–44.

[22] C. Wang et al. "Development of a 3D simulation which can provide better understanding of trainee's performance of the task using airway management training system WKA-1RII". In: *2011 IEEE International Conference on Robotics and Biomimetics*. 2011, pp. 2635–2640.

[23] P. Maiolino et al. "A flexible and robust large scale capacitive tactile system for robots". In: *IEEE Sensors Journal* 13.10 (2013), pp. 3910–3917.

[24] Y. Fei et al. "Risk-Sensitive Reinforcement Learning: Near-Optimal Risk-Sample Tradeoff in Regret". In: *CoRR* abs/2006.13827 (2020). arXiv: 2006.13827.

[25] R Kothari et al. "Time to desaturation in preterm infants undergoing endotracheal intubation". In: 106.6 (2021), pp. 603–607.